Optical spectroscopy of Ce^{3+} in $BaLiF_3$

2000 J. Phys.: Condens. Matter 12 3431

(http://iopscience.iop.org/0953-8984/12/14/318)

J. Phys.: Condens. Matter **12** (2000) 3431–3439. Printed in the UK PII: S0953-8984(00)10978-6

Optical spectroscopy of Ce^{3+} in $BaLiF_3$

M Yamaga†, T Imai†, K Shimamura‡, T Fukuda‡ and M Honda§

† Department of Electrical and Electronic Engineering, Faculty of Engineering, Gifu University, Gifu 501-1193, Japan

‡ Institute for Materials Research, Tohoku University, Sendai 980-8577, Japan

§ Faculty of Science, Naruto University of Education, Naruto 772-8502, Japan

Received 13 January 2000, in final form 18 February 2000

Abstract. The optical absorption spectrum of Ce^{3+} in $BaLiF_3$ crystals consists of several overlapping broad bands. The Ce^{3+} luminescence shows broad bands due to moderate electron–phonon interaction in the 5d excited state. Three distinct Ce^{3+} sites in the crystal were assigned from the optical spectra. The luminescence spectrum from the dominant Ce^{3+} site has a large Stokes shift ($\sim$8300 cm^{-1}), whereas that from one of the two minor Ce^{3+} sites has a Stokes shift of half that magnitude ($\sim$4400 cm^{-1}), assuming that the excitation spectrum is almost the same as for the dominant site. The peaks of the lowest-energy absorption and luminescence bands for the other minor Ce^{3+} site are shifted to lower energy, and the Stokes shift energy ($\sim$7800 cm^{-1}) is close to that for the dominant site. These three Ce^{3+} sites are assigned to configurations of Ce^{3+} accompanied by different charge compensators. This assignment is consistent with preliminary electron spin-resonance results indicating that there exist two tetragonal and two orthorhombic Ce^{3+} centres in the absence of the cubic centre.

1. Introduction

There is much interest in Ce^{3+}-doped ionic crystals for applications in scintillators and tunable lasers [1, 2]. Ce^{3+} ions are represented by a simple one-electron system. The electron configurations of the ground and excited states of Ce^{3+} are $4f^1$ and $5d^1$, respectively. The ^2F_J ground state of $4f^1$ is split by spin–orbit interaction into the $^2F_{5/2}$ and $^2F_{7/2}$ levels, separated by $\sim$2200 cm^{-1}. The ^2D_J excited state of $5d^1$ is affected much more strongly by crystal-field interaction than the ^2F_J state because 5d wavefunctions are somewhat extended towards anion ligands of Ce^{3+}. If the crystal-field interaction for $5d^1$ is much larger than the spin–orbit interaction, then the five degenerate orbital excited states are split into the E_g and T_{2g} states in cubic symmetry and further into five non-degenerate orbital states by a lower-symmetry component.

Optical absorption in Ce^{3+}-doped crystals corresponds to the transitions from the $^2F_{5/2}$ ground state to the five excited states, whereas luminescence occurs as the transitions from the lowest excited state to the $^2F_{5/2}$ and $^2F_{7/2}$ ground states. A moderate electron–phonon coupling for $5d^1$ produces the large energy of the Stokes shift $2S\hbar\omega$ (S: Huang–Rhys factor; $\hbar\omega$: phonon energy) between the absorption and luminescence spectra [3]. In consequence, the absorption spectrum consists of, at most, five overlapping broad bands and the luminescence spectrum has two broad bands with the energy separation of $\sim$2200 cm^{-1}.

The optical absorption and luminescence spectra of the Ce^{3+}-doped fluoride crystals $LiYF_4$ (LYF) [4, 5] and $LiCaAlF_6$ (LiCAF) [6, 7] observed in the UV region are due to Ce^{3+} with S_4 and C_{3v} symmetry, respectively, being substituted at regular sites in these crystals. As

0953-8984/00/143431+09$30.00

energy levels of 5d excited states of Ce^{3+} in crystals are strongly affected by the symmetry and strength of the Ce^{3+} crystal field, optical transitions are assigned to shifts from UV into near-UV regions caused by varying the host crystals [8].

This paper describes the growth of Ce^{3+}-doped single crystals of $BaLiF_3$ (BLF) with symmetry (O_h) different from those of LYF and LiCAF, and characterization of the electronic states of Ce^{3+} in this crystal using optical and electron spin-resonance (ESR) techniques.

2. Experimental procedure

The $BaLiF_3$ (BLF) crystal has the cubic perovskite structure with space group O_h^1, as shown in figure 1. The lattice constant is $a = 3.995$ Å. The polyhedron of Ba^{2+} with the O_h symmetry is composed of twelve F^- ligand ions and eight second-nearest-neighbour Li^+ ions. A Ce^{3+} ion substitutes for a central Ba^{2+} ion, the cerium being accompanied by a nearby charge compensator.

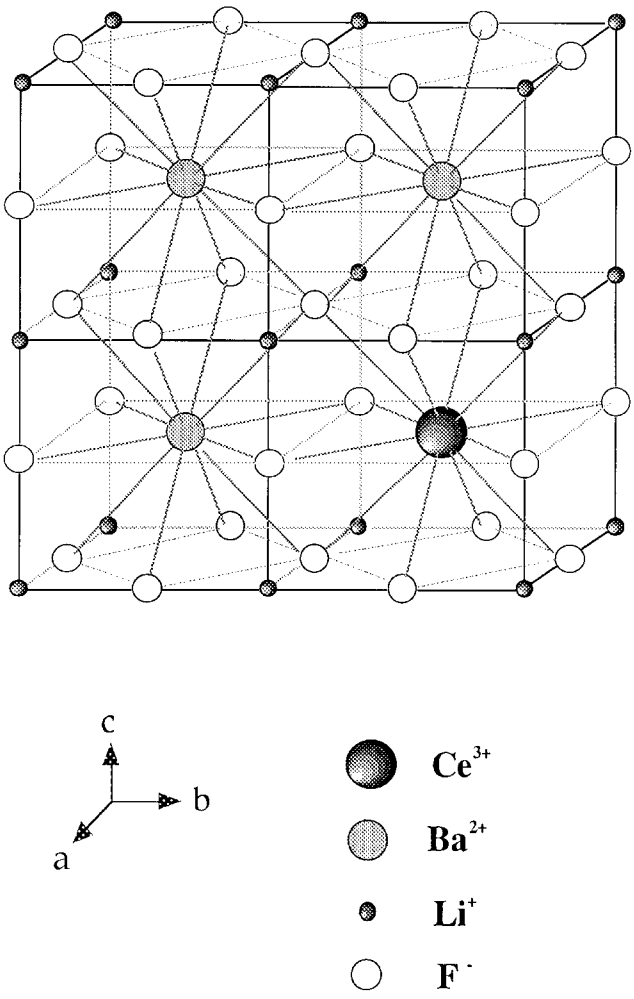

Figure 1. The perovskite crystal structure of $BaLiF_3$.

Crystals of Ce^{3+}-doped BLF were grown in a vacuum-tight Czochralski system equipped with a graphite heater and automatic control of boule diameter. As BLF melts incongruently, a single crystal must be grown from a non-stoichiometric melt to avoid precipitation of other phases. The starting charges were formed from non-stoichiometric mixtures of BaF_2 (43 mol%) and LiF (57 mol%). The compounds were melted and soaked in the furnace for a period of 5 to 6 h under a reactive atmosphere of CF_4. The crystals were grown along the crystalline *c*-axis at a pulling rate of 1 mm h^{-1} and a rotation rate of 15 rpm. After growth, the crystals were gradually cooled down to room temperature; this took about 30 h. The composition, determined by the inductively coupled plasma (ICP) technique, is represented by $Ce_{0.0002}$:$Ba_{0.987}Li_{0.992}F_{2.966}$.

Laue x-ray diffraction was used to produce oriented samples, which were cut parallel to the crystalline *a*-, *b*-, and *c*-axes. These samples were prepared for optical and ESR measurements by polishing their faces using diamond-paste-impregnated laps.

The optical absorption spectra of Ce^{3+} in BLF were measured in the range of 200–2500 nm at room temperature using a Hitachi U-3500 spectrophotometer. The luminescence and excitation spectra were measured in the range of 200–900 nm at room temperature using a Hitachi F-4500 fluorescence spectrophotometer. The lifetime of the Ce^{3+} luminescence was measured using a Horiba NAES-700F time-resolved photoluminescence spectrometer in the temperature range of 77–500 K in the Instrumental Analysis Centre, Gifu University. The ESR measurements were made with a Bruker EMX10/12 X-band spectrometer. The measurements were performed in the temperature range of 5–300 K.

3. Experimental results

Figure 2 shows the absorption spectrum of Ce^{3+} in BLF, which is decomposed into a sum of Gaussians, taking account of the background. This spectrum consists mainly of two spectral

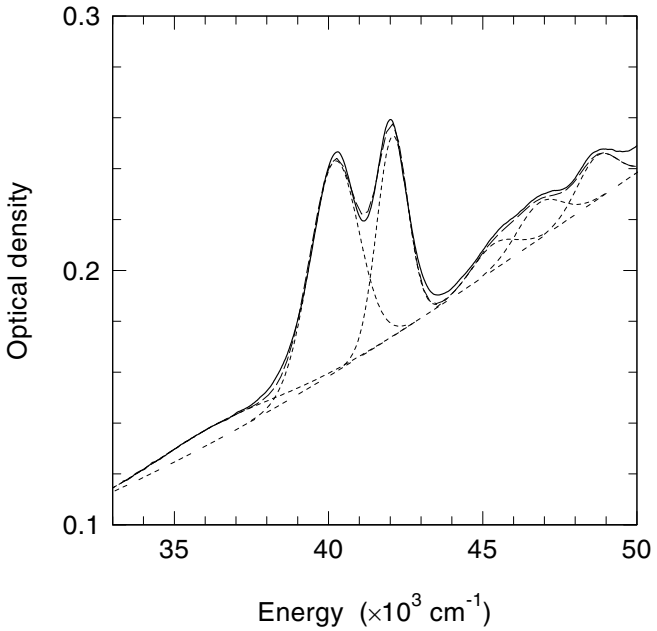

Figure 2. The absorption spectrum of Ce^{3+} in $BaLiF_3$ at room temperature. The spectrum is decomposed into a sum of Gaussians, including the background.

groups, one being two intense bands with peaks at 40 190 and 42 070 cm^{-1}, and the other being three weak bands with peaks at 45 360, 46 840, and 48 720 cm^{-1}. An additional weak band appears at 36 300 cm^{-1} for lower energy.

The UV excitation in the range of 210–260 nm produces a strong luminescence band with a peak at 315 nm denoted by A_1 with a tail to longer wavelengths denoted by A_2 and a very weak band with a peak at 280 nm denoted by C in figure 3(a). New weak bands appear around ∼340 nm when the excitation wavelength is above 270 nm. These bands are denoted by B_1 and B_2. Excitation spectra are obtained by monitoring intensities of luminescence at fixed wavelengths. The excitation spectra were measured in the wavelength range of 280–380 nm as shown in figure 3(b). The excitation spectrum of the A_1 band at $\lambda_{em} = 320$ nm consists of two intense bands with nearly equal intensity and three satellite bands on the side of the shorter wavelength. The features of the absorption, luminescence, and excitation spectra are very similar to those for LYF [4, 5] and LiCAF [6, 7]. These results indicate that the luminescent centre can be assigned to Ce^{3+}. The intensity of the excitation spectrum at $\lambda_{em} = 380$ nm (a tail of the B_2 band to longer wavelengths) is enhanced at ∼207, ∼217, and ∼275 nm. The line shape is different from that at $\lambda_{em} = 320$ nm. The excitation spectrum of the fairly weak C band at $\lambda_{em} = 280$ nm is very similar to that of the A_1 band at $\lambda_{em} = 320$ nm. It is very difficult to distinguish the dominant A_1 and minor C components from the excitation spectra.

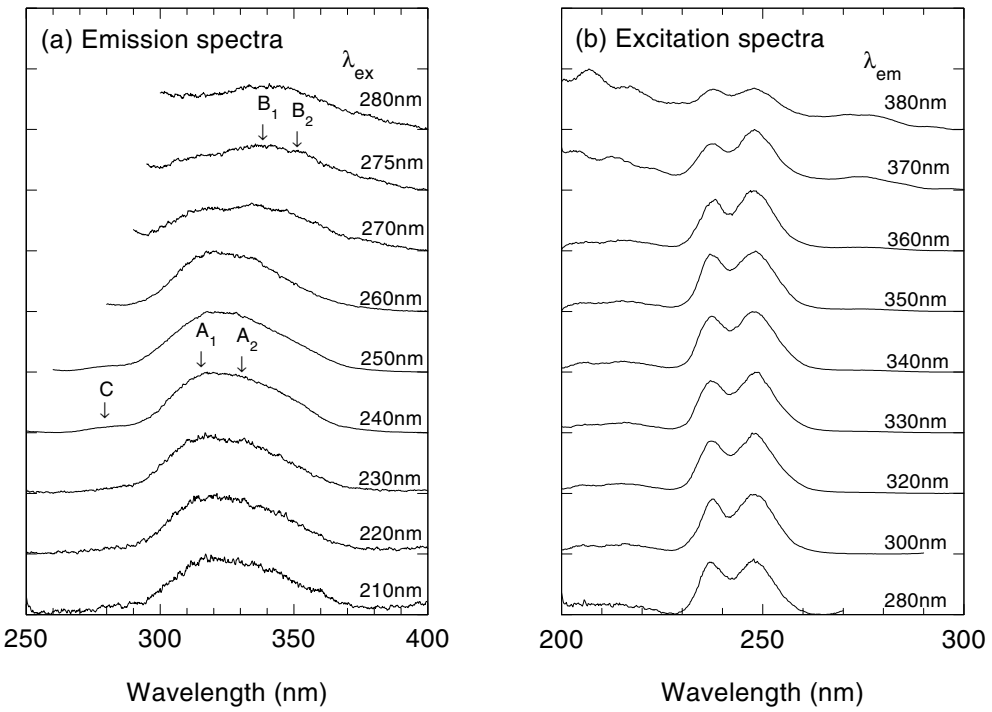

Figure 3. (a) The luminescence spectra of Ce^{3+} in $BaLiF_3$ excited with different wavelengths. The (A_1, A_2), (B_1, B_2), and C bands denote different Ce^{3+} luminescent centres. (b) The excitation spectra obtained by monitoring the intensities of the Ce^{3+} luminescence at different fixed wavelengths.

The Ce^{3+} luminescence spectrum from a single Ce^{3+} site should be decomposed into two Gaussians with the energy separation of 2200 cm^{-1}, which is associated with the transitions from the lowest excited state to the $^2F_{5/2}$ and $^2F_{7/2}$ ground states of Ce^{3+}. In figure 4(a),

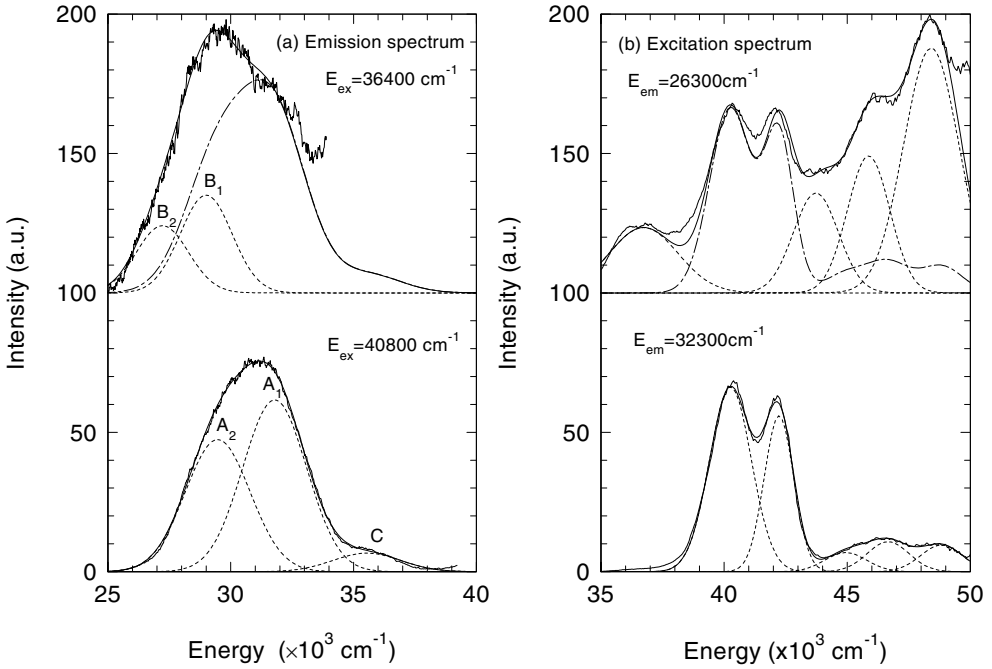

Figure 4. Decomposition of (a) the luminescence spectra and (b) the excitation spectra into Gaussians for $BaLiF_3$:Ce^{3+}. The dashed, dotted–dashed, and solid curves represent each Gaussian component, the sum of Gaussian components of the A configuration, and the total sum of all configurations, respectively.

the calculated curves fit the observed spectra with different excitation energies of 40 800 and 36 400 cm^{-1}, where the horizontal scale is changed from wavelength (nm) to wavenumber (cm^{-1}). The spectrum excited at 40 800 cm^{-1} is decomposed into three Gaussians. The energy separation of the A_1 and A_2 bands is 2000 cm^{-1}. Although a single C band is only observed at high energy, the low-energy component of the C band may overlap the A_1 band. In contrast, additional components B_1 and B_2 of the luminescence with the excitation energy of 36 400 cm^{-1} appear. The components are decomposed into two Gaussians with the assumption that the line-shape parameters of the dominant components A_1 and A_2 do not change, but the relative intensity of the (B_1, B_2) and (A_1, A_2) bands changes as a fitting parameter. The intensities of the higher-energy components for the B configuration may be overestimated due to the background appearing in the high-sensitivity measurement. The energy separation of B_1 and B_2 is estimated to be about 2000 cm^{-1}. In consequence, the (A_1, A_2), (B_1, B_2), and C bands are assigned to three distinct Ce^{3+} centres.

Next, consider the line shapes of the excitation spectra of these Ce^{3+} centres. The excitation spectrum of the A_1 band (32 300 cm^{-1}) in the lower part of figure 4(b) is decomposed into five Gaussians. The line shape is in agreement with the absorption spectrum in figure 2 except the band at 36 400 cm^{-1}. The upper part of figure 4(b) shows the decomposed spectrum at $E_{em} = 26\,300$ cm^{-1}. The excitation spectrum of just the weak B_2 component is obtained by subtracting the spectrum of the A_1 band in the lower part, and represented by a sum of four bands denoted by dashed curves.

Figure 5 shows the decay curves of the Ce^{3+} luminescence measured with fixed excitation and luminescence wavelengths at room temperature. The lifetime (26.4 ns) of the A_1 band

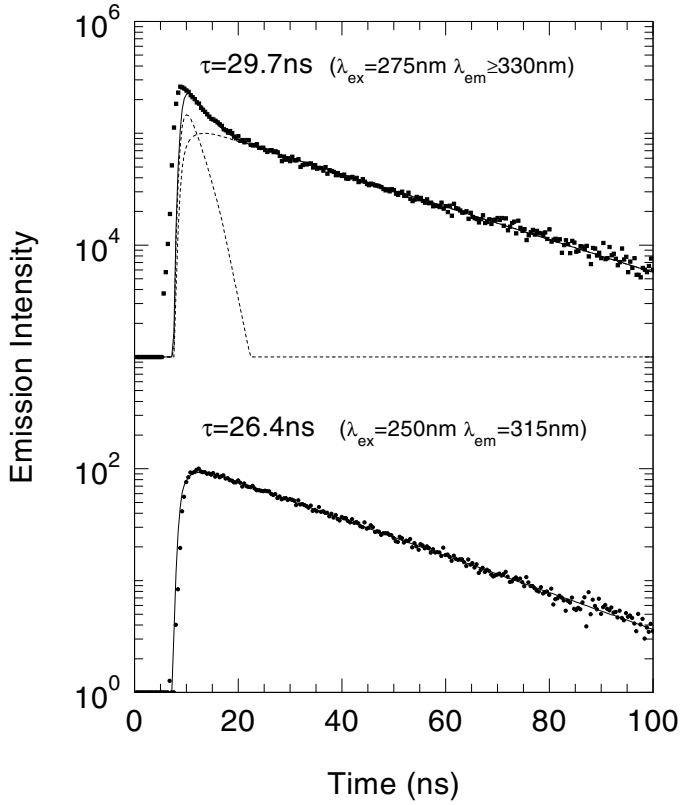

Figure 5. The decay curves of the A_1 luminescence band ($\lambda_{ex} = 250$ nm, $\lambda_{em} = 315$ nm) and the (B_1, B_2) bands ($\lambda_{ex} = 275$ nm, $\lambda_{em} \geqslant 330$ nm). The fast component of the upper figure is due to the scattering of the excitation beam.

is a little shorter than that (29.7 ns) of the (B_1, B_2) bands. Figure 6 shows the temperature dependence of the lifetimes for the A_1 and (B_1, B_2) bands. The lifetime for the A_1 band remains constant below a temperature of 400 K and decreases rapidly above 400 K, whereas that for the B_1 band starts to decrease at 300 K. The temperature dependence of the lifetime is calculated to be of the form of

$$\frac{1}{\tau(T)} = \frac{1}{\tau_r} + \frac{1}{\tau_{nr}} \exp(-\Delta E/kT). \tag{1}$$

The first term contributes to the rate of decay from the electric dipole transition independently of the temperature. The second term is associated with the non-radiative transition to the ground state with the thermal activation energy ΔE. The values of the fitting parameters for the A_1 and (B_1, B_2) bands are obtained as (τ_r, τ_{nr}, ΔE) = (26 ns, 2.5 ps, 3800 cm^{-1}) and (30 ns, 770 ps, 1500 cm^{-1}), respectively.

ESR measurements were made in order to identify Ce^{3+} centres in BLF. Here we describe preliminary results and the details will be reported in a separate paper. The ESR spectra observed at low temperatures are assigned to four distinct Ce^{3+} centres: two distinct tetragonal Ce^{3+} centres distorted along the [001] axis and two distinct orthorhombic centres distorted along the [110] axis in the absence of the cubic centre. These results indicate that the Ce^{3+} centres are accompanied by different charge compensators, which are strongly associated with third-nearest-neighbour Ba^{2+} sites along the [001] and [110] axes.

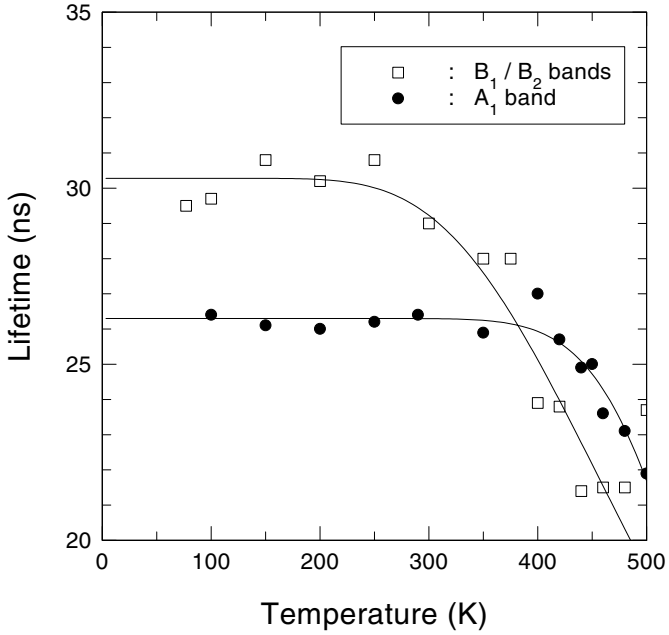

Figure 6. The temperature dependence of the lifetimes of the A_1 and (B_1, B_2) luminescence bands. Solid curves are calculated using equation (1) and the parameters (τ_r, τ_{nr}, ΔE) = (26 ns, 2.5 ps, 3800 cm^{-1}) and (30 ns, 770 ps, 1500 cm^{-1}) for the A_1 and (B_1, B_2) luminescence bands, respectively.

4. Discussion

The optical transition energy of Ce^{3+} is determined by the symmetry and strength of the Ce^{3+} crystal field in ionic crystals. First, consider the energy levels of Ce^{3+} ions in octahedral and cubic symmetries, which are sixfold and eightfold coordinated to anion ligands, respectively. The ^2D excited state splits into the E_g and T_{2g} orbital states in O_h symmetry. The lowest excited state is T_{2g} and E_g for the octahedron and cube, respectively. This result is confirmed by the observed absorption spectra of the Ce^{3+} octahedron with the C_{3v} symmetry in LiCAF [7] and of the Ce^{3+} cube with the C_{4v} symmetry in $LiYbF_4$ [9].

The Ce^{3+} cubo-octahedron in BLF consists of twelve F^- ligands classified as two groups, one containing eight ligands in a cube and the other containing four ligands in an octahedron that lacks the two ligands on the crystalline *c*-axis. As the crystal-field splittings of the ^2D excited state in the cube and octahedron are in opposite senses, these two components of the crystal field in BLF compete with each other, so the crystal-field splitting in BLF is expected to be small relative to those in oxide and fluoride crystals with different symmetry [8]. This is consistent with the small separations between the five absorption bands of Ce^{3+} in BLF observed in figure 2. The absorption spectrum also indicates that the lower excited state of Ce^{3+} in BLF is the E_g state, which is further split into A_1 and B_1 states by the lower-symmetry component—for example, a tetragonal distortion.

We consider the configurations of the three distinct Ce^{3+} centres corresponding to the (A_1, A_2), (B_1, B_2), and C luminescence bands, denoted simply as A, B, and C, respectively. The absorption and excitation spectra for the A configuration reflect the cubo-octahedron symmetry with a small separation between T_{2g} and E_g excited states, whereas the luminescence

has a large Stokes shift energy ($\sim$8300 cm^{-1}) [10]. This value is much larger than those for $LiYbF_4$ ($\sim$3100 cm^{-1}) [9] and LiCAF ($\sim$2600 cm^{-1}) [7]. Marsman *et al* calculated the 4f and 5d energy levels of Ce^{3+} accompanied by various charge compensators using an *ab initio* chemical cluster calculation method [11]. According to their calculations, the substitution of a Li^+ ion for a Ba^{2+} ion along the [001] axis induces a fairly large Stokes shift because the large space near the Ce^{3+} ion causes the large lattice relaxation in the 5d excited state. This configuration is confirmed by the ESR result that cubo-octahedra axially distorted along the [001] axis were observed. In consequence, the A configuration is assigned to the substitution of a Li^+ ion for the Ba^{2+} ion along the [001] axis.

Let us consider the C configuration, whose Stokes shift energy ($\sim$4400 cm^{-1}) is half that of the A configuration and whose excitation spectrum seems to be similar to that of the A configuration. As the absorption and excitation spectra are due to the transitions between the ground and excited states with the same configuration coordinate, the crystal field of the C configuration may be very close to that of the A configuration. Taking into account the ESR result that orthorhombic Ce^{3+} centres with [110]-axis distortions were observed, the most probable charge compensation is the substitution of a Li^+ for a Ba^{2+} along the [110] axis. However, the distance between Ce^{3+} and Ba^{2+} along the [110] axis is $\sqrt{2}$ times larger than that along the [001] axis, as shown in figure 1. The longer distance is less effective as regards the lattice relaxation in the lowest 5d excited state. In consequence, the Stokes shift energy for the C configuration is expected to be smaller than that for the A configuration.

Next, we discuss the B configuration in which the peak energies of the lowest-energy absorption and luminescence bands are shifted to lower energy. One possible mechanism is a Ba^{2+} vacancy on the [001] or [110] axis. Such a vacancy produces much larger distortion than the substitution. As the distortion further splits the 5d excited states, the lowest excited state is shifted to lower energy. This model is also supported by the ESR results indicating that the other tetragonal and orthorhombic centres with larger distortions along the [001] and [110] axes were observed at low temperatures.

Finally, the relation between the lifetime and the configuration is discussed. The B-configuration lifetime (30 ns) is larger than the A-configuration lifetime (26 ns). As the increase of the lifetime corresponds to the decrease of the spin-allowed 5d $\rightarrow$ 4f electric dipole transition probability, the wavefunction of the 5d orbital is expected to expand toward the ligands, or the p states of the central Ce^{3+} and ligand F^- ions to be mixed into the lowest 5d excited state through odd-parity distortions. The odd distortions are produced more effectively by the vacancies of Ba^{2+} ions along the [001] and [110] axes than by the substitution of a Li^+ ion for a Ba^{2+} ion. The shift of the lowest 5d excited state to lower energy for the B configuration enhances the non-radiative decay rate associated with tunnelling between the excited- and ground-state potential wells. This is consistent with the fact that the temperature ($\sim$300 K) at which the B-configuration lifetime starts to decrease is lower than that for the A configuration.

5. Conclusions

The absorption, luminescence, and excitation spectra observed for the Ce^{3+}-doped BLF crystal are assigned as due to three distinct Ce^{3+} centres. As Ce^{3+} ions substitute for Ba^{2+} ions, an excess charge of +1 should be compensated for. The proposed charge-compensation mechanisms for the Ce^{3+} centres are (i) the substitution for Ba^{2+} ions along the [001] and [110] axes with Li^+ ions and (ii) vacancies of Ba^{2+} ions along the [001] and [110] axes. These configurations can explain the energy levels, relaxation energy, and lifetime of the 5d excited states for the three Ce^{3+} centres observed in the BLF crystal.

Acknowledgments

This work was partially supported by the Research for the Future Programme 'Growth and characterization of single crystals for active elements' of the Japan Society for the Promotion of Science. One of the authors (M Yamaga) is indebted to Corning for a Research Grant Award.

References

[1] Moulton P 1985 *Laser Handbook* vol 5, ed M Bass and M H Stitch (Amsterdam: North-Holland) p 282
[2] Blasse G and Grabmaier B C 1994 *Luminescent Materials* (Berlin: Springer)
[3] Henderson B and Imbusch F G 1989 *Optical Spectroscopy of Inorganic Solids* (Oxford: Clarendon) ch 5
[4] Ehrlich T D J, Moulton P F and Osgood R M 1978 *Opt. Lett.* **4** 184
[5] Okada F, Togawa S and Ohta K 1994 *J. Appl. Phys.* **75** 49
[6] Marshall C D, Speth J A, Payne S A, Krupke W F, Quarles G J, Castillo V and Chai B H T 1994 *J. Opt. Soc. Am.* B **11** 2054
[7] Yamaga M, Lee D, Henderson B, Han P T J, Gallagher H and Yosida T 1998 *J. Phys.: Condens. Matter* **10** 3223
[8] Kodama N, Yamaga M and Henderson B 1998 *J. Appl. Phys.* **84** 5820
[9] Verweij J W M, Pedrini C, Bouttet D, Dujardin C, Lautesse H and Moine B 1995 *Opt. Mater.* **4** 575
[10] Combes C M, Dorenbos P and van Eijk C W E 1995 *J. Lumin.* **72–74** 753
[11] Marsman M, Andriessen J and van Eijk C W E 1999 *Int. Conf. on Luminescence and Optical Spectroscopy of Condensed Matter (Osaka, 23–27 August 1999)* collected abstracts PC1-11